Materials and Structures (2017) 50:21
DOI 10.1617/s11527-016-0930-5

ORIGINAL ARTICLE

Moment-axial force domain of corroded R.C. columns

G. Campione · F. Cannella · L. Cavaleri · M. F. Ferrotto

Received: 24 February 2016 / Accepted: 8 July 2016 / Published online: 10 August 2016

Abstract In the present paper, a simple model to determine the moment-axial force domain of the cross-section of reinforced concrete (R.C.) columns subjected to corrosion process is presented. The model considers members with square and rectangular cross-sections and it accounts for—cover spalling; buckling of longitudinal reinforcing bars; loss of bond of bar in tension; reduction of confinement pressures (due to the reduction of the area of stirrups and cracking of concrete induced by rust formation). The analytical expressions for prediction of the area reduction of steel, bond strength and critical load of longitudinal bars utilized were verified against experimental data available in the literature. Ample verification of the analytical model proposed for prediction of moment-axial force domain was made against available experimental data given in the literature, showing good agreement. Finally, the proposed model gives simple expressions for a preliminary static check on existing cross-sections of R.C. columns subjected to corrosion processes.

Keywords Moment-axial forces domain · Confinement · Buckling · Corrosion · Cover spalling

G. Campione (✉) · F. Cannella · L. Cavaleri · M. F. Ferrotto
DICAM, University of Palermo, Viale Delle Scienze, Palermo 90128, Italy
e-mail: giuseppe.campione@unipa.it

List of symbols

a	Shear span
A_{l}	Area of all longitudinal bars
$A_{\mathrm{l,red}}$	Reduced area of all longitudinal bars
$A_{\mathrm{f,red}}$	Reduced area of longitudinal bars in a layer (tension or compression)
A_{p}	Area of pit
A_{st}	Area of stirrup
$A_{\mathrm{s,red}}$	Reduced area of corroded reinforcement
$A_{\mathrm{st,red}}$	Reduced area of corroded stirrup
$A_{1\mathrm{c}}$	Unconfined concrete cover area
$A_{2\mathrm{c}}$	Confined cracked concrete of the core area across the bars
$A_{3\mathrm{c}}$	Internal area of concrete core
b	Width of column
c_{cA}	Position of neutral axis in case of point A
c_{cB}	Position of neutral axis in case of point B
c_{cu}	Position of neutral axis in case of flexure
d	Effective depth
e	Eccentricity
E_{p}	Hardening modulus of steel
E_{r}	Reduced elastic modulus of steel
E_{s}	Elastic modulus of steel
f_{c}	Compressed strength of concrete
f_{c}^{*}	Reduced compressed strength of concrete
f_{cc}	Compressed strength of confined concrete
f_{ct}	Tensile strength of concrete
f_{le}	Confinement pressure
f_{y}	Yield stress of reinforcement bar
k	Coefficient related to the calculus of ψ

H Height of column
I Inertia moment of a bar
I_{red} Reduced inertia moment of a bar
I_{st} Inertia moment of a stirrup
i_{corr} Corrosion current density
k_l Distributed stiffness parameter for a corner or mid-face bar
k_q Empirical constant
L Length of beam of experimentation
M Bending moment on the column
M_A Bending moment in point A
M_B Bending moment in point B
m_B Dimensionless bending moment in point B
M_f Point of pure bending
m_f Dimensionless moment related to the point of pure bending
M_u Ultimate moment associated with the design axial force N
m_u Dimensionless ultimate moment associated with the design axial force N
M_{uc} Moment capacity for compression failure
M_{us} Ultimate flexural strength
n Number of longitudinal bars
n_{bars} Number of bars in compressed zone
N Axial force on the column
N_A Axial force in point A
n_A Dimensionless axial force in point B
N_B Axial force in point B
n_B Dimensionless axial force in point B
N_c Point of pure compression
n_c Dimensionless point of pure compression
$p(t)$ Depth of pit
p_{max} Maximum depth of pit
p_{av} Average depth of pit
q_{res} Bond strength in presence of corrosion
q_0 Bond strength without corrosion
R Pitting factor
s Spacing of stirrup
s_1 Spacing of laterally supported longitudinal reinforcement
t Time
X Thickness of the corrosion attack penetration
X_p Loss of mass
β Reduction factor of the yielding stress
γ Reduction factor of bond strength
δ Concrete cover
ε_0 Strain of concrete
λ Empirical constant
μ Empirical constant
v_{rs} Ratio of volumetric expansion of the oxides with respect to the virgin material
ρ Geometrical ratio of steel
σ_{cr} Maximum stress in a bar due to buckling effect
σ_s Available stress in the stirrups
ϕ_l Diameter of uncorroded bar
$\phi_{l,red}$ Reduced diameter of corroded bar
ϕ_{st} Diameter of uncorroded stirrup
ϕ_0 Diameter of uncorroded bar/stirrup
ψ Reduction factor of the compressed concrete
ω_b Mechanical ratio of steel

1 Introduction

It is widely accepted that general and pitting corrosion of reinforcement affects reinforced concrete (R.C.) structures by reducing the cross-sectional area and the mechanical properties of the reinforcement itself, especially when pitting corrosion occurs. Pitting is a localized corrosion type. By contrast, general corrosion is distributed along the bars. Moreover, loss of bond between the steel and concrete and cracking of concrete in the zone of rust formation cause a reduction in the strength and stiffness of the reinforced concrete members.

Based on the literature review [1–6], it could be seen that individual aspects of reinforced concrete element deterioration are well covered. In addition, literature related to evaluation of the load carrying capacity of deteriorated reinforced concrete columns subjected to axial force and to axial force and bending moment is available [7–17]. More work is required to develop a suitable and simple methodology for strength evaluation of deteriorated reinforced concrete columns that incorporates all corrosion-related factors and deterioration scenarios.

For concrete columns cover spalling, buckling of steel bars, reduction of steel area due to rust formation and in some cases opening of the stirrups are the main visible effects due to corrosion.

Experimental researches [8, 9] have been carried out in an attempt to understand the behavior and bearing capacity of corroded R.C. columns. Also, some in situ long term investigations are available [17]. At present few simple analytical and numerical models have been developed and calibrated with the experimental results

to predict the bearing capacity of the moment-axial force domain of corroded R.C. columns [11, 13].

In this paper, the effects of reinforcement corrosion, loss of concrete cover, and loss of bond on the structural behavior of R.C. columns with rectangular cross-section are quantified. Moment-axial force domains (M–N) using a simplified model are proposed and verified against experimental data available in the literature.

2 Research significance

The main object of the present research is to propose a simple model for calculation of the moment-axial force domain of rectangular or square cross-sections of R.C. corroded columns. Instead of utilizing a numerical procedure based on the layer method, an analytical model is proposed which only considers the case of pure compression, pure bending and a point having the same bending moment of pure flexure and the axial force to be determined and finally a point equal to half of the previous case and a bending moment to be determined. The main phenomena due to loss of bond, buckling of longitudinal bars, loss of confinement effect due to rust formation and reduction of compressive strength induced by concrete cracking are included in the model. The range of study cases was that in which buildings were only designed for gravity loads in which the beams were designed with the scheme of continuous beams for gravity loads and the columns were designed for gravity loads considered as isolated members.

3 Moment-axial forces domain

The cases examined are those shown in Fig. 1. They refer to short R.C. members having rectangular (or square) cross-sections with side b and height H and reinforced with n longitudinal steel bars with diameter ϕ_l and area A_l, and confined by transverse closed steel stirrups with diameter ϕ_{st} and area A_{st}. Transverse steel is placed in the plane of the cross-section at clear spacing s with a cover δ. In the case of bars distributed up to four layers of reinforcement, an equivalent area of main bars was considered applied to the center of the bar in tension and in compression.

Figure 2 shows the moment-axial force domain of the transverse cross-section obtained numerically

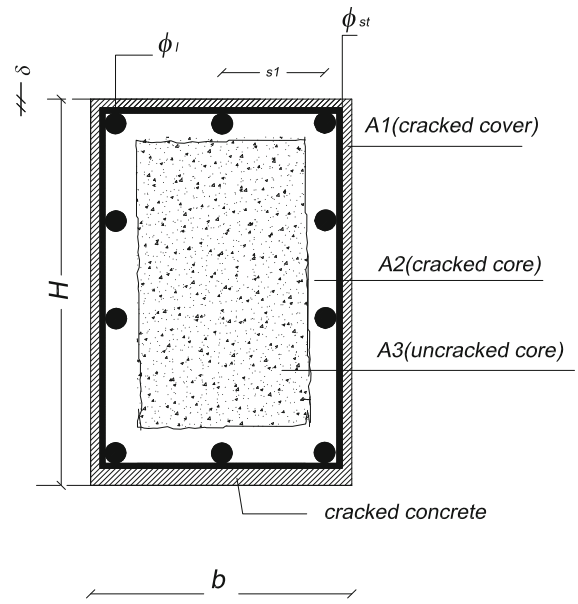

Fig. 1 Cross-sections analyzed

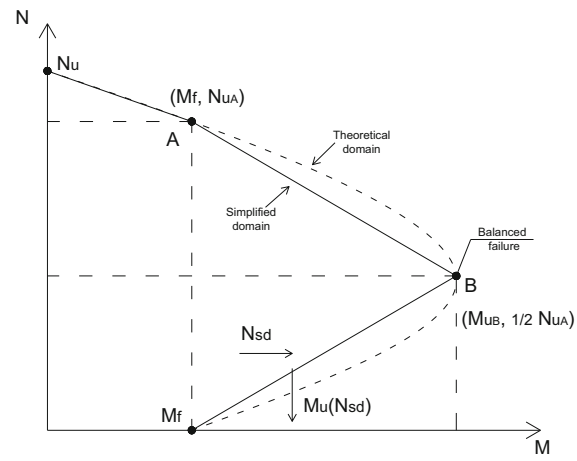

Fig. 2 Moment-axial force domain

using the layer method and indicated with the dashed line. In the same graph the continuous line also shows the simplified model adopted here [18]. This model considers three linear branches: the first one connects the point of pure compression N_c with the point A, the second branch is the segment A-B and the third branch connects B with the point of pure bending M_f. Point A corresponds to a point having the same bending moment of pure flexure M_f and the axial force equal to N_A to be determined. Point B is characterized by an axial force $N_B = 0.5 \cdot N_A$ and a bending moment M_B to be determined. Figure 2 shows the simplified

linearized moment-axial force domain fitting the ones obtained numerically. In the next section details for calculation of single points of the interaction diagram are given.

3.1 Case of pure compression

As suggested in Campione et al. [16], the load-carrying capacity of corroded compressed R.C. columns (see Fig. 1) can be determined as the sum of the four different strength contributions due to: the unconfined concrete cracked cover area (A_{1c}), the confined cracked concrete of the core area across the bars (A_{2c}), the internal area of concrete core which is in a triaxial stress state (A_{3c}), the longitudinal bars $A_{l,red}$ including buckling phenomena.

The expression that gives the load-carrying capacity in compression for the case of a member with a rectangular cross-section is the following:

$$\begin{aligned} N_u =& \psi \cdot f_c' \cdot \left[(2 \cdot b \cdot \delta + 2 \cdot H \cdot \delta) - 2\delta^2\right] \\ &+ \psi \cdot f_{cc} \cdot \{b \cdot H - [(2 \cdot b \cdot \delta + 2 \cdot H \cdot \delta) \\ &- 2\delta^2] - [(b - 2 \cdot \delta - 2 \cdot \varphi_{st} - 2 \cdot \varphi_l) \\ &\cdot (H - 2 \cdot \delta - 2 \cdot \varphi_{st} - 2 \cdot \varphi_l)]\} \\ &+ f_{cc} \cdot [(b - 2 \cdot \delta - 2 \cdot \varphi_{st} - 2 \cdot \varphi_l) \\ &\cdot (H - 2 \cdot \delta - 2 \cdot \varphi_{st} - 2 \cdot \varphi_l)] + \beta \cdot \left(A_{l,red} \cdot f_y\right) \end{aligned} \quad (1)$$

f_{cc} being the compressive strength of the confined concrete, ψ a reduction factor of the compressed concrete in the zone of rust formation and β the reduction factor of the yielding stress of the longitudinal bars due to a buckling effect.

The reduction in ψ, as suggested in Coronelli et al. [19], can be calculated by considering that the cracking induced by the expansion of the corroded longitudinal and transverse steel bars (rust effect) degrades the strength of the compressed concrete because of the increase in cracking. If the lateral strain, which causes longitudinal micro-cracks, is assumed to be smeared on the cracks, we have:

$$\psi = \frac{f_c^*}{f_c} = \frac{1}{1 + k \cdot \frac{2 \cdot \pi \cdot n_{bars} \cdot (\nu_{rs} - 1) \cdot X}{b \cdot \varepsilon_0}} \quad (2)$$

with $k = 0.1$ as suggested in Coronelli et al. [19], and ε_0 assumed 0.002 for normal strength, normal weight concrete.

X is the thickness of the corrosion attack penetration, which can be measured with the gravimetric method or calculated, as suggested in Val [4], in a rearranged form of Faraday's law of electrolysis, as:

$$X = 0.0116 \cdot i_{corr} \cdot t \quad (3)$$

where i_{corr} is the corrosion current density in the reinforcing bar expressed in $\mu A/cm^2$ and t the time in years.

The compressive strength f_{cc} of the confined concrete was calculated as in Razvi et al. [20] in the form:

$$\frac{f_{cc}}{f_c} = 1 + 6.7 \cdot \left(\frac{f_{le}}{f_c}\right)^{-0.17} \quad (4)$$

with the confinement pressure f_{le} calculated as in [20], but taking into account, as in Campione et al. [16], that if corrosion processes are present the confinement pressure has to be reduced. This reduction is due to the reduction of the area of transverse steel bars and to the available stress in the stirrup due to rust formation. It also has to be stressed that although it is true that the expansion of rusted material produces premature loading on the stirrups, we also know that preloading should confine the concrete surrounded by stirrups and longitudinal reinforcement. This effect was not considered in the paper, also because at ultimate stress the concrete cover is spalled off and the longitudinal bars buckle.

The effective confinement pressures prove to be:

$$\begin{aligned} f_{le} =& \left(\frac{2 \cdot A_{st,red} \cdot \sigma_s}{b \cdot s}\right) \\ &\times \left(0.15 \cdot \sqrt{\frac{b}{s} \cdot \frac{b}{s_1} \cdot \left(\frac{2 \cdot A_{st,red} \cdot \sigma_s}{b \cdot s}\right)}\right) \end{aligned} \quad (5)$$

where $A_{st,red}$ is the reduced area of the stirrups, σ_s the available stress in the stirrups, and s_1 the spacing of the laterally supported longitudinal reinforcing.

Considering the free expansion of the side of the cross-section due to rust formation in the external bars and, consequently, the elongation of the stirrup, the stress in the stirrup proves to be:

$$\sigma_s = f_y \cdot \left[1 - \frac{2 \cdot X}{b} \cdot \frac{E_s}{f_y}\right] \quad (6)$$

The reduction of the stirrup area due to rust formation and pitting, if it occurs, can be derived, as in [16], in the form:

$$A_{st,red}(t) = n_{bar} \cdot \left\{ \frac{\pi \cdot [\varphi_1 - 2 \cdot X]^2}{4} - A_p(t) \right\} \quad (7)$$

A_p, as is shown in Fig. 3, is the cross-sectional area of pitting calculated with the expression in [4], as:

$$A_p(t) = \begin{cases} A_1 + A_2 & p(t) \le \frac{\varphi_0}{\sqrt{2}} \\ \frac{\pi \cdot \varphi_0^2}{4} - A_1 + A_2 & \frac{\varphi_0}{\sqrt{2}} \le p(t) \le \varphi_0 \\ \frac{\pi \cdot \varphi_0^2}{4} & p(t) \ge \varphi_0 \end{cases} \quad (8)$$

In Eq. (7) the parameters to be calibrated are R and X. The reduction of ϕ and A_p is a consequence.

To calibrate these parameters, the data in [9] were utilized, as shown in Fig. 4.

In [9] all reinforcements of five sets of simply supported beams, with cross-sections having $b = 150$ mm, $H = 200$ mm and $L = 2300$ mm, were corroded, inducing general and pitting corrosion, by applying a current of 100 μA/cm^2. The amount of corrosion was determined by weight loss, while the pitting depths were measured. Two-point loading was applied at an a/d ratio of 4.6. Figure 4 shows the comparison between experimental data from [9] versus analytical attack penetration of the steel area due to corrosion. It is important to underline the weight of the R factor: the presence of pitting reduces the area of the bar by about 20 %. The best fit of the experimental results was obtained assuming $R = 3$ and assuming Eq. (3) to be valid.

$$A_1 = \frac{1}{2} \times \left[2 \cdot \arcsin\left(\frac{2 \cdot p(t) \cdot \sqrt{1 - \left(\frac{p(t)}{\varphi_0}\right)^2}}{\varphi_0} \right) \cdot \left(\frac{\varphi_0}{2}\right)^2 - 2 \cdot p(t) \cdot \sqrt{1 - \left(\frac{p(t)}{\varphi_0}\right)^2} \cdot \left| \frac{\varphi_0}{2} - \frac{p(t)^2}{\varphi_0} \right| \right] \quad (9)$$

$$A_2 = \frac{1}{2} \times \left[2 \cdot \arcsin\left(\frac{2 \cdot p(t) \cdot \sqrt{1 - \left(\frac{p(t)}{\varphi_0}\right)^2}}{2 \cdot p(t)} \right) \cdot \left(\frac{\varphi_0}{2}\right)^2 - 2 \cdot p(t) \cdot \sqrt{1 - \left(\frac{p(t)}{\varphi_0}\right)^2} \cdot \frac{p(t)^2}{\varphi_0} \right] \quad (10)$$

The depth of pit $p(t)$ can be evaluated as:

$$p(t) = 0.0116 \cdot i_{corr} \cdot t \cdot R \quad (11)$$

According to Val [4] $R = p_{max}(t)/p_{av}(t)$ values are between 4 and 10 for 5 and 10 mm reinforcing bars of length 150–300 mm.

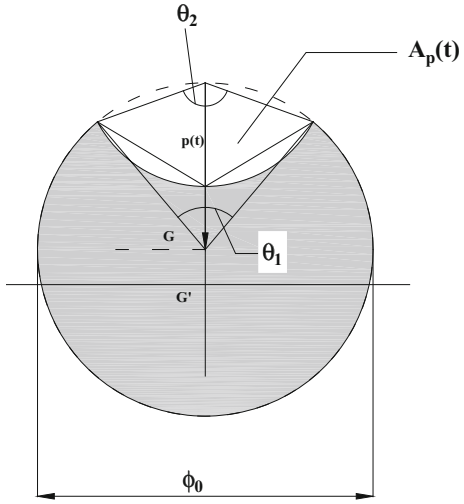

Fig. 3 Pitting attack in a reinforcing bar according to the model given in [4]

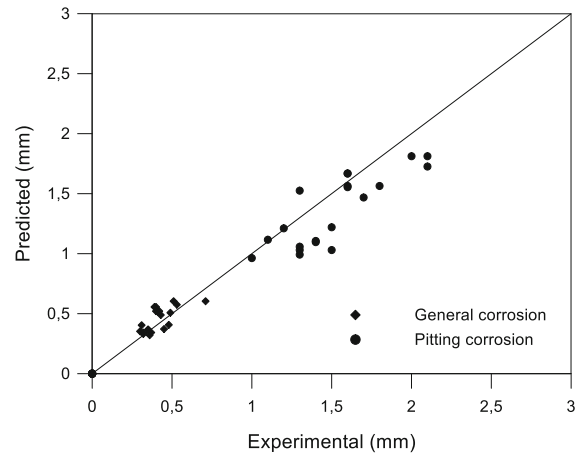

Fig. 4 Experimental versus theoretical reduction in bar section

Figure 5 shows the reduction in the area of the bars with time, increasing for cases of general corrosion and general corrosion and pitting; $R = 3$ and $i = 0.5$ and 1 μA/cm^2 were chosen as examples. Comparison shows that, with a service life of 50 years, the reduction of the area of the bars is between 30 and 10 % with and without pit, respectively.

It has to be stressed that, as is well known from the literature [21–24], there is no significant reduction of yielding stress due to corrosion processes. Apostolopoulos et al. [21], Fernandez et al. [22, 23] and Biondini et al. [24]) show that, with an increase in the corrosion level, the yield stress of the bar decreases slowly (less than 15 %). In almost all cases, failure of the bar is due to the presence of a brittle region owing to the presence of pitting. Otherwise, the presence of pitting causes a reduction of the ductility of the bars, as can be seen in Stewart [25].

For longitudinal compressed bars, if the concrete cover is spalled off due to rust formation, the risk of buckling increases. In this case, the maximum allowable stress in the longitudinal bars is the minimum among the yielding stress and the critical stress. The latter can be calculated, as in [16], in the form:

$$\sigma_{cr} = \frac{3.46 \cdot \sqrt{E_r \cdot I \cdot k_l}}{A_l} \left(\mathrm{N/mm^2}\right) \tag{12}$$

$$E_r = \frac{4 \cdot E_s \cdot E_p}{\left(\sqrt{E_s} + \sqrt{E_p}\right)^2} \tag{13}$$

with

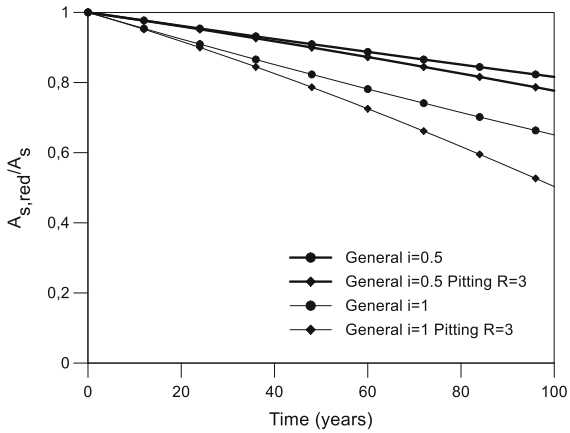

Fig. 5 Normalized reduction of steel area with time increase

$$I = \frac{\pi \cdot \varphi_l^4}{64} \tag{14}$$

and E_p the hardening modulus of steel and k_l a distributed stiffness parameter in the form:

$$k_l = \frac{E_P \cdot A_{st}}{b \cdot s} \cdot \sqrt{2} \tag{15}$$

for a corner bar and

$$k_l = \frac{48 \cdot E_P \cdot I_{st}}{s_l^3 \cdot s} \text{for a mid} - \text{face bar} \tag{16}$$

with $I_{st} = \frac{\pi \cdot \varphi_{st}^4}{64}$ and $A_{st} = \frac{\pi \cdot \varphi_{st}^2}{4}$.

Finally, the reduction factor β of the yield stress in the longitudinal bar due to buckling can be defined as $\beta = \frac{\sigma_{cr}}{f_y}$.

Under corrosion, Eqs. (12, 14, 15, 16) are still utilized adopting the area and the diameter of bars deduced with Eq. (7). If corrosion is due to a pitting effect, the moment of inertia has to be modified (see Fig. 3). If we refer to the model in [4], the moment of inertia of the cross-section of the bars subjected to pitting has the following expression:

$$\begin{aligned} I_{red} = {} & \frac{\pi \cdot \varphi_l^4}{64} - \frac{\pi \cdot \varphi_l^2}{4} \cdot \frac{A_p(t)}{\frac{\pi \cdot \varphi_l^2}{4} - A_p(t)} \cdot \frac{2}{3} \cdot \frac{\varphi_l}{2} \cdot \frac{\sin\left(\frac{\theta_l}{2}\right)}{\frac{\theta_l}{2}} \\ & - \frac{1}{4} \cdot \left(\frac{\varphi_l}{2}\right)^4 \cdot \left[\frac{\theta_l}{2} + 0.5 \cdot \sin(\theta_l)\right] \\ & + \left[\frac{\pi \cdot \varphi_l^2}{4} \cdot \frac{A_p(t)}{\frac{\pi \cdot \varphi_l^2}{4} - A_p(t)} - \frac{2}{3} \cdot \frac{\varphi_l}{2} \cdot \frac{\sin\left(\frac{\theta_l}{2}\right)}{\frac{\theta_l}{2}}\right]^2 \cdot A_p(t) \end{aligned} \tag{17}$$

The use of Eq. (17) is quite complex. A simplification can be obtained numerically by deriving from Eq. (17) the diameter of an equivalent bar having the same inertia, giving the following expression:

$$\frac{\varphi_{l,red}}{\varphi_l} = 1 + 0.0029 \cdot X_p - 0.003 \cdot X_p^2 \tag{18}$$

with X_p the loss of mass in (%).

Figure 6 gives experimental results for compressed bars having pitting corrosion. Then a comparison between the analytical results (Eq. 12) and experimental results is given. The scatter between the analytical and experimental results is in the range of 10 %. The data utilized [6] refer to compressive tests on single bars with different s/ϕ_l ratios and different levels of loss of mass. The comparison shown in Fig. 6

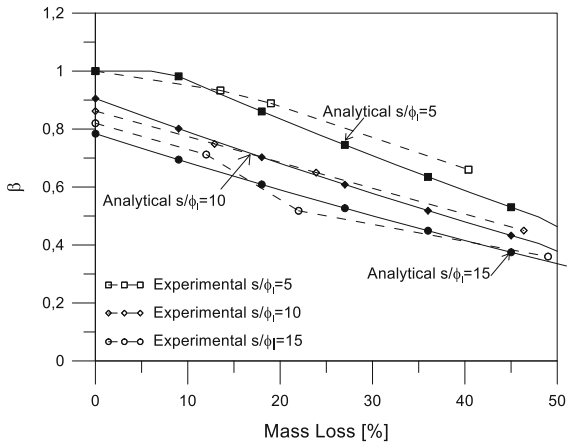

Fig. 6 Normalized reduction of yielding stress in compressed bar with loss of mass in %

highlights that in most of the cases examined the model captures the experimental results, emphasizing the importance of including the pitting attack for calculation of the reduced moment of inertia of the cross-section of longitudinal bars.

3.2 Case of flexure

The reference model for prediction of the flexural strength of an uncorroded R.C. section is based on the hypothesis that the plane section theory is applied because of a perfect bond between bars and concrete. In the case of corroded bars, slippage between concrete and steel bars occurs, reducing the strength and the available ductility. Moreover, it has to be stressed that pitting is a localized corrosion type. By contrast, general corrosion may be evident during inspection. Therefore, in the analytical model pitting effects should be analysed by considering probabilistic distribution (position of pitting and effect on single bars). The current model refers to a sectional analysis.

To reproduce the worst condition, it was supposed that pitting and general corrosion occur in all bars and in a section where these effects are very important. This case could be representative of the anchorage zone of longitudinal bars of columns or in zones where high shear forces are present. Moreover, the model is valid only for sections with all reinforcement corroded. Studies in the literature [11–14] analyse cases in which the corrosion level is different along the four sides of the cross-section. The case examined here is the one of greatest interest because it represents the worst condition.

To include the slippage of longitudinal bars due to rust formation a reduction factor γ of the yielding stress of longitudinal bar was introduced. Uniform reduction of the yielding stress of longitudinal bars between two successive flexural cracks was supposed.

The γ factor is defined here as the ratio between the bond strength of the corroded bars and the bond strength of the uncorroded bars.

The expression utilized is the one given in [8] in the form:

$$q_{res} = 0.6 \cdot \left(0.5 + \frac{\delta}{\varphi_l}\right) \cdot f_{ct} \cdot (1 - \lambda \cdot X^{\mu}) + \frac{k_q \cdot A_{st} \cdot f_y}{s \cdot \varphi_l} \quad (19)$$

with f_{ct} the tensile strength of the concrete expressed as a function of the characteristic compressive strength f_{ck} in Eurocode 2 [26] as:

$$f_{ct} = 0.30 \cdot f_{ck}^{2/3} (\text{MPa}) \quad (20)$$

k_q, μ, λ being empirical constants. According to Rodriguez et al. [8], k_q and μ are equal to 0.16, 0.1 respectively, while λ is between 0.26 and 0.4 and assumed here to be 0.4.

In the absence of stirrups, assuming $d = \varphi_l$ Eq. (19) gives a reduction factor of bond strength in the form:

$$\gamma = \frac{q_{res}}{q_o} = \frac{1}{1 + \frac{\frac{k_q \cdot A_{st} \cdot f_y}{s \cdot \varphi_l}}{0.18 \cdot \left(0.5 + \frac{\delta}{\varphi_l}\right) \cdot f_c^{\frac{2}{3}}}} \left[(1 - \lambda \cdot X^{\mu}) + \frac{\frac{k_q \cdot A_{st} \cdot f_y}{s \cdot \varphi_l}}{0.18 \cdot \left(0.5 + \frac{\delta}{\varphi_l}\right) \cdot f_c^{\frac{2}{3}} \cdot} \right] \quad (21)$$

with X related to X_p through the expression:

$$X_p = 1 - \left(1 - \frac{2 \cdot X}{\varphi_l}\right)^2 \quad (22)$$

Figure 7 shows the experimental results available in the literature [27, 28] and the analytical prediction with Eq. (21). The comparison between the literature results and the analytical ones shows good agreement. It has to be stressed that, for the purposes of this paper, Fig. 8 shows only the post-peak branch because we

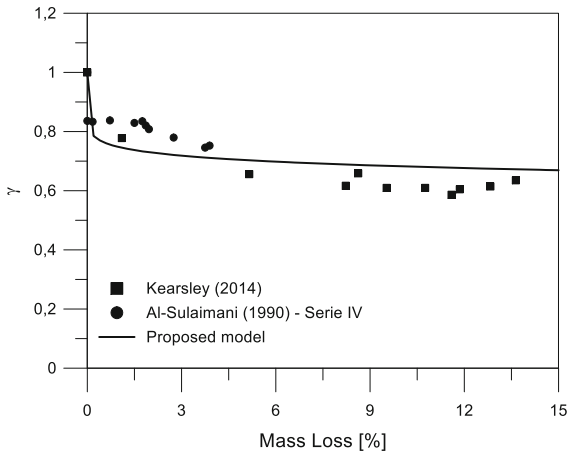

Fig. 7 Experimental versus theoretical dimensionless bond strength reduction

refer to the ultimate state of columns with severe corrosion levels.

As can be seen in Fig. 8, the position of the neutral axis c_{cu} and the ultimate flexural strength M_{us} are in the form:

$$c_{cu} = \frac{A_{f,red} \cdot (\gamma - \beta) \cdot f_y}{0.85 \cdot f_{cc} \cdot 0.80 \cdot b} \tag{23}$$

$$M_f = A_{f,red} \cdot (\gamma + \beta) \cdot f_y \cdot (d - \delta) - \frac{1}{2} \cdot A_{f,red} \cdot \gamma \cdot f_y \cdot (\varphi_l + 0.80 \cdot c_{cu}) \tag{24}$$

with $d = H - \phi_{st} - \phi_l/2$ and $A_{f,red}$ the reduced area both in tension and in compression.

In Eqs. (23, 24) the γ coefficient was introduced to take bond degradation into account.

The flexural strength should also not exceed the moment capacity M_{uc} for compression failure of corroded beams [29], calculated as:

$$M_{uc} = 0.125 \cdot \psi \cdot f_c \cdot b \cdot \left(d - \delta - \frac{\varphi_l}{2}\right)^2 \tag{25}$$

3.3 Case of axial force and bending moment

With reference to the simplified moment-axial force domain in Fig. 2 it is possible to obtain the point coordinate of A by solving the following translational and rotational equilibrium equations:

$$N_A = 0.85 \cdot c_{cA} \cdot b \cdot 0.80 \cdot f_{cc} + A_{f,red} \cdot (\beta - \gamma) \cdot f_y \tag{26}$$

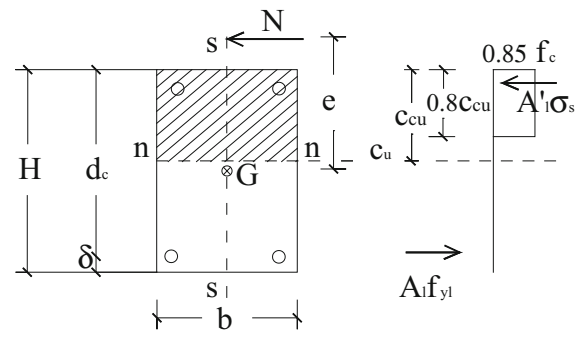

Fig. 8 Design assumptions for analysis of single R.C. column

$$\begin{aligned} M_A &= N_A \cdot e \\ &= (0.85 \cdot f_{cc} \cdot 0.80 \cdot c_{cA} \cdot b) \\ &\quad \times \left(\frac{H}{2} - \delta - 0.4 \cdot c_{cA}\right) + A_{f,red} \cdot (\beta + \gamma) \cdot f_{yl} \\ &\quad \times \left(\frac{H}{2} - \delta - \frac{\varphi_l}{2}\right) \end{aligned} \tag{27}$$

By imposing $M_A = M_f$ and solving Eq. (27) with respect to c_{cA}, a second-degree equation is obtained that if solved gives c_{cA}. Substituting the value of c_{cA} in Eq. (26) gives N_A.

Point B in the interaction diagram corresponds to the so-called balanced failure condition. This point is known to be located around $0.4 - 0.6 \cdot A_c \cdot f_c$. However, it depends very much on the reinforcement arrangement. Nevertheless, it is possible to derive rational equations based on plane strain distributions. In this paper the coordinate of point B of Fig. 2 was obtained following the procedure proposed in Bergmann et al. [18] and Eurocode 4 [30] in which was set $N_B = 0.5\ N_A$. The position of the neutral axis, under these hypotheses, is equal to:

$$c_{cB} = \frac{0.5 \cdot N_A + A_{f,red} \cdot f_y(\gamma - \beta)}{0.8 \cdot f_{cc} \cdot b} \tag{28}$$

and the ultimate moment was obtained from Eq. (27) with substitution of Eq. (28)

$$\begin{aligned} M_B &= (0.85 \cdot f_{cc} \cdot 0.80 \cdot c_{cB} \cdot b) \\ &\quad \cdot \left(\frac{H}{2} - \delta - 0.4 \cdot c_{cB}\right) + A_{f,red} \cdot f_{yl} \\ &\quad \cdot \left(\frac{H}{2} - c - \frac{\varphi_l}{2}\right) \cdot (\gamma + \beta) \end{aligned} \tag{29}$$

The ultimate moment associated with the design axial force N can be calculated in the following form:

$$M_{\mathrm{u}}(N) = M_{\mathrm{u}} + N \cdot \left(\frac{M_{\mathrm{B}} - M_{\mathrm{u}}}{N_{\mathrm{B}}} \right) \quad \text{with} \quad N \leq N_{\mathrm{B}} \tag{30}$$

or in dimensionless form

$$m_u(n) = \frac{M_u(N)}{b \cdot d_c^2 \cdot f_c} = m_u + \frac{n}{n_B} \cdot (m_B - m_u) \quad \text{with} \quad n \leq n_B \tag{31}$$

4 Experimental validation

The data in [11–14] referring to members with square or rectangular sections were utilized in order to validate the proposed model.

Tapan and Aboutaha [11] analyzed one column with a cross-section of width 1350 mm and height 1830. The longitudinal reinforcement was constituted by nine 36-mm bars for each side with a cover equal to 80 mm. The stirrups, constituted by deformed bars, had a diameter of 12 mm. The authors considered six deterioration cases with two lengths of exposed bars: case I shows a column with corrosion at the extreme compression layer of the bars; case II analyzes a column with corrosion of the extreme tension layer of the bars; case III refers to a column with corroded extreme left or side bars; case IV shows all bars corroded; - case V analyzes a column with corrosion at the extreme compression layer of the bars and the left side bars; case VI refers to a column with corroded bars at the extreme tension layer and the left side. For each case, five levels of mass loss of reinforcement were taken into account: 0, 4.25, 10, 50 and 75 %. In this paper, only the results of case IV are compared with the proposed model.

Figure 9 shows the moment-axial force domain obtained with the proposed model and with the numerical procedure indicated in [11]. The comparison is quite satisfactory for the case of flexure and pure compression, while in the case of bending moment and axial force the proposed model slightly overestimated the numerical results with scatter within 5 %.

Wang et al. [12] analyzed a column with a square cross-section of side 610 mm. The longitudinal

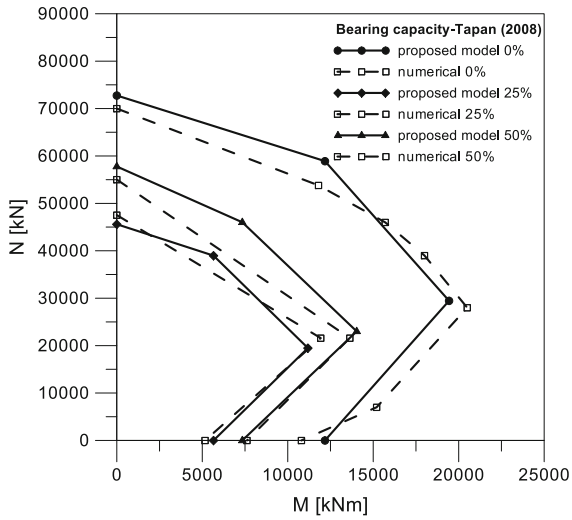

Fig. 9 Comparison between analytical and experimental interaction diagrams

reinforcement was constituted by four 28-mm bars for each side, with a cover of 28 mm. The stirrups were constituted by 12-mm bars with a pitch equal to 250 mm. The authors considered six deterioration cases: case I shows a column with corrosion at the extreme compression layer of the bars; case II analyzes a column with corrosion of the extreme tension layer of the bars; case III refers to a column with corroded extreme left or side bars; case IV shows all bars corroded; case V analyzes a column with corrosion at the extreme compression layer of the bars and the left side bars; case VI refers to a column with corroded bars at the extreme tension layer and the left side. For each case, five levels of loss of mass of reinforcement were taken into account: 0, 4.25, 10, 50 and 75 %. In this paper, only the results of case IV are compared with the proposed model.

Figure 10 shows the moment-axial force domain obtained with the proposed model and with the numerical procedure indicated in [12]. The comparison is also satisfactory in this case. For a loss of mass of 50 % the scatter is higher and in the range of 15 % for compression.

Figures 9 and 10 clearly also show that for the case in [11] with the increase in the loss of mass the load-carrying capacity decreases significantly. For 10 and 25 % the reduction of axial load is almost 35 and 60 %. In flexure, similar results are obtained. For the case in [12] the analogous decrements of load-carrying capacity for 25 and 50 % of loss of mass were 20 and

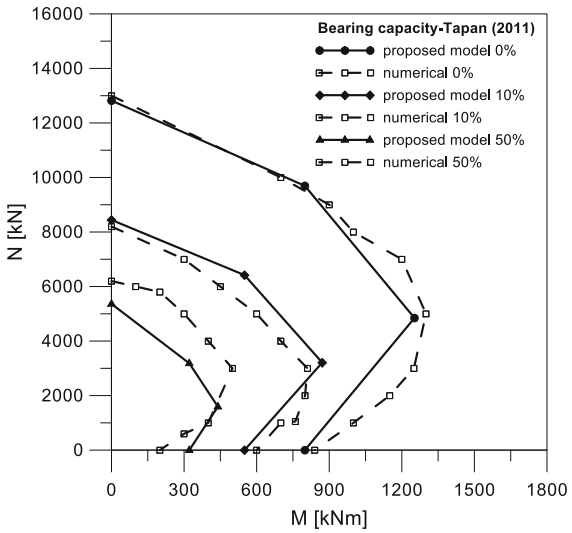

Fig. 10 Comparison between analytical and experimental interaction diagrams

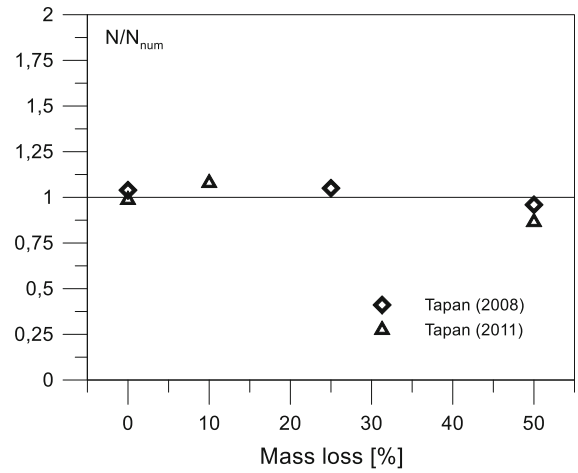

Fig. 11 Comparison between analytical and numerical ultimate axial force

39 %, while in flexure they were 38 and 58 %. It is important to stress that if the buckling effect and loss of bond are neglected the reduction of load-carrying capacity and flexural capacity can be addressed only to the area reduction of the steel bars and to the cover spalling, but it gives unsafe results.

For analyses of experimental results, it has to be stressed that failure was controlled by bar buckling, bond deterioration and concrete strength degradation. More specifically, in the case of flexure bond, degradation and buckling of longitudinal bars are the most important phenomena governing failure, while in the case of compression, buckling and reaction of concrete strength were the main phenomena covering the problem. In the case of axial force and bending moment all phenomena occur but for $N < N_B$ buckling and bond failure are predominant, while for $N > N_B$ concrete strength reduction plays an important role too.

Figure 11 shows for the case of pure compression the ratio between the analytical and numerical results given in [11, 12] for different losses of mass, highlighting the good agreement between the numerical and the analytical prediction.

Tapan and Aboutaha [13] tested twelve columns with a square cross-section of side 200 mm. T longitudinal reinforcement was constituted by four 18-mm deformed bars, one in each corner with a 30-mm cover. The stirrups, constituted by deformed bars, had a diameter of 8 mm and pitch equal to 100 mm. Specimens were corroded by adding 3.5 % of calcium chloride ($CaCl_2$) and by connecting the tensile bars with a DC power supply. The columns were tested with two different types of eccentric distances (Type ZX with small eccentricity and Type ZD with large eccentricity), two different positions of the corroded zone (Type L corresponding to a corroded tensile zone and Type Y to a corroded compressed zone) and different types of corrosion levels that were defined in terms of average weight loss of the steel. There were three columns with a high corrosion level (ZDL700-2, ZDL350-3 and ZDY350-3), two with a low level (ZDL700-1 and ZDY700-1) and others with intermediate values.

Guo et al. [14] tested four columns with cross-section having width equal to 600 mm and height 250 mm. The longitudinal reinforcement was constituted by twelve 16-mm bars, with a cover thickness of 25 mm. The stirrups, constituted by deformed bars, had a diameter of 8 mm and spacing of 150 mm. Corrosion was induced by applying a current to the longitudinal and transverse reinforced bars of each specimen, which was enclosed in a brick tank filled with 3.5 % NaCl solution. Four specimens were tested, with a different level of corrosive damage, calculated as mass loss of the longitudinal reinforcement: 0, 5, 10 and 15 % for specimen 1, 2, 3 and 4, respectively. The effects of accelerated corrosion were cracks at the corners of the specimen due to corrosion and volume expansion of the corrosion product of the longitudinal rebar and the stirrups.

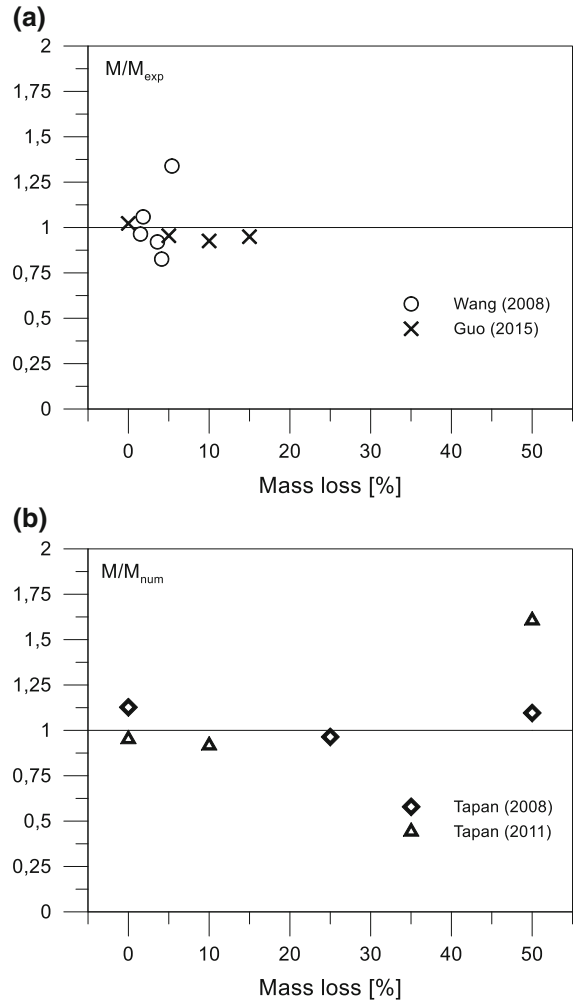

Fig. 12 Comparison between analytical and **a** experimental ultimate bending moment **b** numerical ultimate bending moment

Figure 12a, b shows for the case of flexure under constant axial force the ratio between analytical and experimental results given in [11, 14] for different loss of mass, highlighting the good agreement for almost all cases examined between numerical and analytical prediction. Similarly, Fig. 13 shows for the case of balanced failure the ratio between analytical and experimental results given in [11, 12] for different loss of mass highlighting the good agreement between numerical and analytical prediction.

5 Practical considerations and suggestions

In this section, dimensionless equations are derived and numerical examples are given.

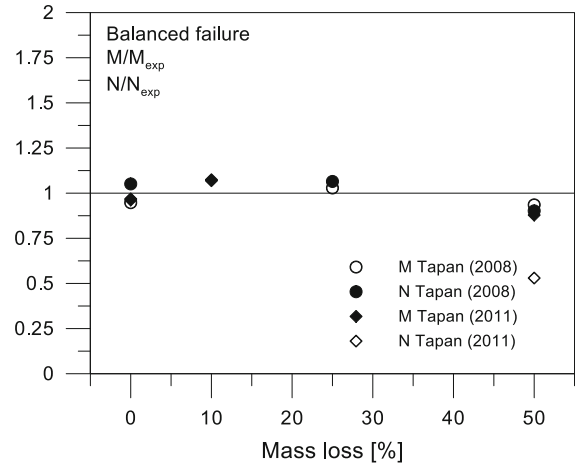

Fig. 13 Comparison between analytical and experimental ultimate axial force bending moment

The diagrams obtained here are derived dimensionless. They can be useful to reuse when typical cases of existing corroded structures designed for gravity load have to be verified. In these cases, if the loss of mass is known they give the reduction in the load-carrying capacity of columns under bending moment and axial force. Of course in all other cases the dimensionless moment-to-axial force domain has to be derived.

A rearranged form of Eq. (1) and Eqs. (26–31) for rectangular cross-sections in a simplified dimensionless form, in which terms of one order lower were neglected, is the following:

$$n_c = \frac{N_c}{b \cdot H \cdot f_c} = 1 + 0.2 \cdot (\psi - 0.05) + \beta \cdot \omega \qquad \omega = \frac{A_{s,red} \cdot f_y}{b \cdot H \cdot f_c} \tag{32}$$

$$m_f = \frac{M_f}{b \cdot d^2 \cdot f_c} = \gamma \cdot \omega \cdot \left(0.92 - \frac{\delta}{d}\right) \tag{33}$$

$$0.272 \cdot \left(\frac{c_{cA}}{d}\right)^2 - 0.68 \cdot \left(\frac{b - 2\delta}{2 \cdot d}\right) \cdot \frac{c_{cA}}{d} - 0.5 \cdot \omega \cdot \beta \cdot \left(\frac{b - 2\delta}{2 \cdot d}\right) + m_f = 0 \tag{34}$$

$$n_A = 0.68 \cdot \frac{c_{cA}}{d} + \frac{\omega}{2} \cdot \beta \tag{35}$$

$$n_B = \frac{n_A}{2} \tag{36}$$

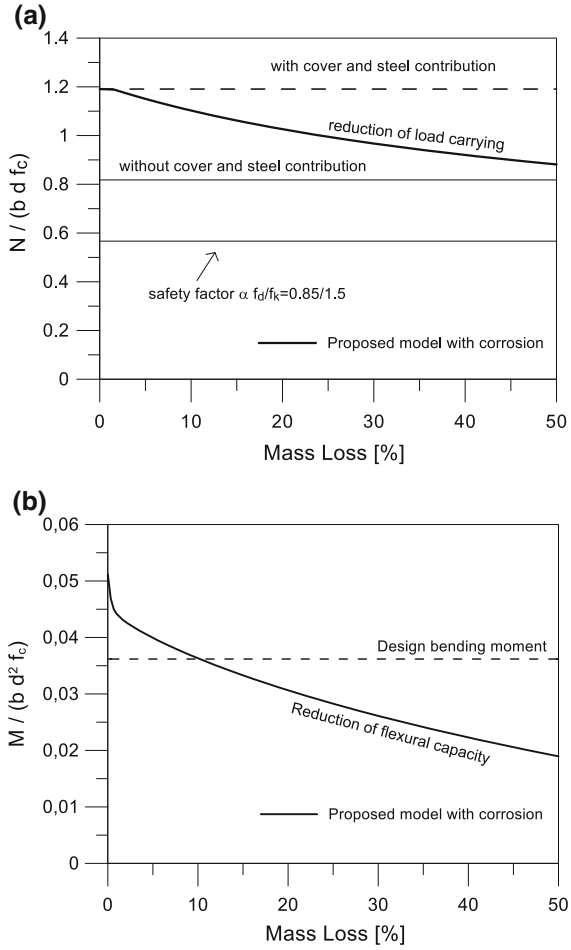

Fig. 14 Dimensionless diagram of: **a** axial forces versus loss of mass; **b** bending moment versus loss of mass

$$\frac{c_{cB}}{d} = \frac{n_A - 0.5 \cdot \omega \cdot (\beta - \gamma)}{0.68} \tag{37}$$

$$m_B = 0.68 \cdot \frac{c_{cA}}{d} \cdot \left(\frac{b - 2\delta}{2 \cdot d} - 0.4 \cdot \frac{c_{cA}}{d} \right) + 0.5 \cdot \omega \cdot \left(\frac{b - 2\delta}{2 \cdot d} \right) \cdot (\beta + \gamma) \tag{38}$$

The numerical example refers to a square cross-section of side $b = H = 400$ mm, with cover $d = 30$ mm, reinforced with four longitudinal bars for each layer having diameter 14 mm and stirrups having diameter 8 mm at pitch 200 mm. The concrete had $f_c = 15$ MPa and the yielding of the steel was $f_y = 220$ MPa.

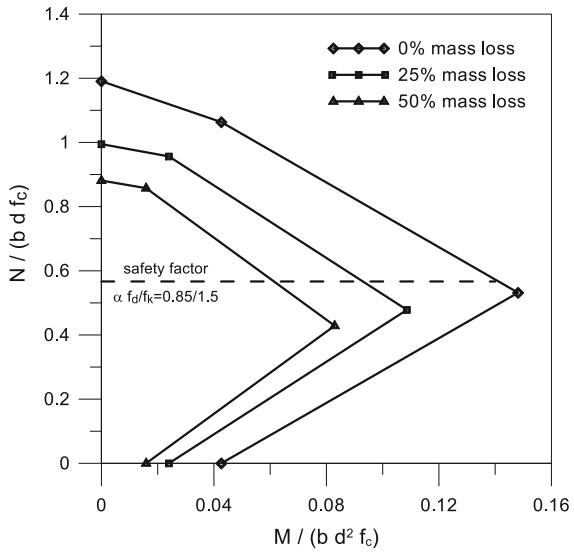

Fig. 15 Dimensionless diagram of axial force-bending moment versus loss of mass

Figure 14a, b gives the variation in dimensionless axial force and bending moment with the loss of mass. Figure 14a also indicates the safety factor for the concrete, which according to Eurocode 2 [26] is equal to 0.47. It also gives the strength contribution calculated without considering loss of mass for cases including cover and longitudinal bars and cases neglecting both. The comparison shows that even for high levels of loss of mass, the load-carrying capacity of the columns is higher than the safety factor; therefore, the loss of mass does not significantly affect the safety factor of the column. By contrast, in flexure (Fig. 14b) it is shown that a sudden loss of load-carrying capacity occurs due to the effects of both loss of area and loss of bond. Since beams are generally designed for maximum strength with ductile behavior the steel contribution in tension governs the behavior in flexure and the maximum design moment (e.g. 0.04 in Fig. 14b) is very close to the strength of the section. Therefore, even with a loss of mass of 25 % the reduction in load-carrying capacity is almost 46 % and the safety factor margin is exceeded.

Figure 15 shows the dimensionless moment-axial force domains for two different levels of loss of mass. In the same graph the value of the dimensionless axial force, equal to 0.47, corresponding to the design strength of the concrete in compression, is also shown. With the corrosion process increasing the strength of the cross-section decreases with a significant loss of

moment capacity for the same level of axial force. For a loss of mass of 25 and 50 % the loss of moment capacity is 29 and 43 % respectively.

It has to be stressed that the authors compare the global safety margin with the concrete strength reduction factor for new constructions. It also has to be emphasized that the analysis is not general, as the actual safety margin will also depend on the safety factor of the steel, which will be different for different steel reinforcement ratios. In the case presented here, that is of great interest because existing structures designed in the last few decades for gravity loads the steel ratio was very low, so the results are likely to be less dependent on steel corrosion than in other cases. Therefore, lower safety factors for assessment should be utilized.

6 Conclusions

In the present paper, a simplified model to calculate the moment-axial force domain of R.C. corroded columns subjected to corrosion processes was developed and verified against selected experimental data.

The simplified domain is constituted by three branches and four points. To take into account loss of load-carrying capacity due to corrosion processes, the model considers: cover expulsion; cracking of the portion of confined core close to the longitudinal bars and stirrups; reduction of steel area; buckling of compressed reinforcement; loss of bond of tensile reinforcement.

The limitations of the proposed model, which covers several cases of practical interest, are mainly that the following: the corrosion process of bars involves them in the same manner; cover spalling occurs along the four sides of the section.

The main results obtained can be summarized as follows:

The reduction in the load-carrying capacity due to loss of mass of longitudinal bars is not relevant for compressed members designed for static loads;

The reduction in the load-carrying capacity is between 20 and 30 % for severe corrosion conditions because of degradation of the compressive strength of the outer portion of the column.

In flexure, loss of bond plays a fundamental role with respect to loss of area, and loss of mass of 15–20 % produces a loss of strength of 30–40 %.

Under an axial load and bending moment, the reduction of flexural capacity depends on the loss of area of the reinforcement (longitudinal and stirrups) and of the loss of bond and buckling of compressed bars in which pitting plays an important role.

For low levels of axial force, the main effect is the loss of flexural capacity, which in the case of a loss of mass of 25 % can produce a reduction of up to 45 %.

Further cases to be confirmed experimentally referring to higher steel ratios will be investigated in the future to cover these cases too.

References

1. Tuutti K (1982) Corrosion of steel in concrete. Fo 4.82, Swedish Cement and Concrete Research Institute, Stockholm, Sweden
2. Cairns JA, Plizzari GA, Du Y, Law D, Franzoni C (2005) Mechanical properties of corrosion-damaged reinforcement. ACI Mater J 102(4):256–264
3. Cairns JA, Du Y, Law D (2007) Influence of corrosion on the friction characteristics of the steel/concrete interface. Constr Build Mater 21:190–197
4. Val DV (2007) Deterioration of Strength of RC Beams due to Corrosion and Its Influence on Beam Reliability. ASCE J Struct Eng 133(9):197–1306
5. Wang X, Liu X (2004) Modeling bond strength of corroded reinforcement without stirrups. Cem Conc Res 34: 1331–1339
6. Kashani MW, Crewe AJ, Alexander NA (2013) Nonlinear stress-strain behavior of corrosion-damaged reinforcing bars including inelastic buckling. Eng Struct 48:417–429
7. Uomoto T, Misra S (1990) Behavior of concrete beams and columns in marine environment when corrosion of reinforcing bars takes place. Concr Marine Environ ACI SP 109–6:127–146
8. Rodriguez J, Ortega L, Garcia A (1994) Corrosion of reinforcing bars and service life of R/C structures: corrosion and bond deterioration. Proc Int Conf Concr Across Bord 2:315–326
9. Rodriguez J, Ortega LM, Casal J (1996) Load carrying capacity of concrete structures with corroded reinforcement. Constr Build Mater 11(4):239–248
10. Bae SW, Belarbi A, Myers JJ (2005) Performance of corrosion-damaged RC columns repaired by CFRP sheets. ACI Spec Publ 230(82):1447–1464
11. Tapan M, Aboutaha RS (2008) Strength evaluation of deteriorated RC bridge columns. J Bridge Eng 13(3): 226–236
12. Wang XH, Liang FY (2008) Performance of RC columns with partial length corrosion. Nucl Eng Des 238(12): 3194–3202
13. Tapan M, Aboutaha RS (2011) Effect of steel corrosion and loss of concrete cover on strength of deteriorated RC columns. Constr Build Mater 25:2596–2603

14. Guo A, Li H, Ba X, Guan X, Li H (2015) Experimental investigation on the cyclic performance of reinforced concrete piers with chloride-induced corrosion in marine environment. Eng Struct 105:1–11
15. Jayant J, Arora HC, Sharma UK (2015) Structural performance of differently confined and strengthened corroding reinforced concrete columns. Constr Build Mater 82:287–295
16. Campione G, Cannella F, Minafo G (2016) A simple model for the calculation of the axial load-carrying capacity of corroded RC columns. Mater Struct 49:1935–1945
17. Ismail M, Muhammad M, Ismail ME (2010) Compressive strength loss and reinforcement degradations of reinforced concrete structure due to long-term exposure. Constr Build Mater 24:898–902
18. Bergmann R, Matsui C, Meinsma C, Dutta D (1995) Design guide for concrete filled hollow section columns under static and seismic loading. Verlag TUV Rheinhald, Cologne
19. Coronelli D, Gambarova P (2004) Structural assessment of corroded reinforced concrete beams: modeling guidelines. ASCE J Struct Eng 130(8):1214–1224
20. Razvi S, Saatcioglu M (1999) Confinement model for high-strength concrete. J Struct Eng ASCE 125(3):281–288
21. Apostolopoulos CA, Papadakis VG (2008) Consequences of steel corrosion on the ductility properties of reinforcement bar. Constr Build Mater 22:2316–2324
22. Fernandez I, Bairàn JM, Marì AR (2015) Corrosion effects on the mechanical properties of reinforcing steel bars. Fatigue and σ-ε behavior. Constr Build Mater 101:772–783
23. Fernandez I, Bairàn JM, Marì AR (2016) Mechanical model to evaluate steel reinforcement corrosion effects on σ-ε and fatigue curves. Experimental calibration and validation. Constr Build Mater 118:320–333
24. Biondini F, Vergani M (2015) Deteriorating beam finite element for nonlinear analysis of concrete structures under corrosion. Struct Infrastruct Eng 11(4):519–532
25. Stewart MG (2009) Mechanical behavior of pitting corrosion of flexural and shear reinforcement and its effect on structural reliability of corroding RC beams. Struct Saf 31:19–30
26. Eurocode 2: Design of concrete structures, EN-1992-1-1 (2004)
27. Al-Sulaimani GJ, Kaleemullah M, Basunbul IA, Rasheeduzzafar (1990) Influence of corrosion and cracking on bond behavior and strength of reinforced concrete members. ACI Struct J 87(2):220–231
28. Kearsley EP, Joyce A (2014) Effect of corrosion products on bond strength and flexural behavior of reinforced concrete slabs. J South Afr Inst Civil Eng 56(2):21–29
29. MacGregor JG (1997) Reinforced concrete: Mechanics and design, 3rd edn. Prentice-Hall, Upper Saddle River
30. Eurocode 4: Design of composite steel and concrete structures. EN 1994-1-1 (2004)